JOURNAL OF SOLID STATE CHEMISTRY 23, 191–204

Structures Related to the β-Tungsten or Cr_3Si Structure Type

STEN ANDERSSON

Chemical Center, Division of Inorganic Chemistry 2, University of Lund, Lund, Sweden

Received April 25, 1977; in revised form July 5, 1977

Using traditional crystallographic operations such as translation, rotation and reflection, and intergrowth, it is shown how several structures, among them the tetrahedrally close-packed, can be accurately derived from the β-tungsten structure type. Examples are Zr_4Al_3, Fe_2B, Mo_3CoSi, Ga_2Mg_5, GaMg, Ga, α- and β-V_3S, W_2CoB_2, CeAl, W_5Si_3, the σ-phase, the Friauf–Laves phases, the μ-phase, the *P* and *M* phases, the $(Co_{0.57}Si_{0.43})_3V_2$ phase, the χ-phase, and the ν-phase.

When a crystal of a complex structure is formed, we like to think that nature starts by building a unit of a simple structure. We imagine, for various chemical reasons, that these units are then joined together at the atomic level in ways that can be described by (a) crystallographic operations (translation, rotation, reflection) and (b) intergrowth. The geometry of these operations was recently described in a review article (*1*). In the final structure, the simple unit often retains infinite extension in one or two dimensions. Considerable confidence in this theory has been accumulated through the years from indirect evidence; it is possible to describe and classify an increasing number of complex structures using these crystal building principles. For example, the structures of many transition-metal oxides and oxide fluorides could be described with the building-block principle (*2*, *3*) and the intergrowth model (*4*). Such structures were once characterized as *predictable* (*5*), they were superficially very complex, but once the simple units were recognized, the structures could easily and accurately be described in simple terms. Experiments showed that some of the complex oxides in the MoO_3–Nb_2O_5 system were formed very fast and easily (*6*), but direct evidence did not exist for the proposed general thought.

When a crystal grows, nature makes its faux pas in the form of mistakes or defects. The character of such faux pas is of course directly dependent on the structure building principle. Using electron microscopy, Allpress and co-workers (*7*) managed to resolve and determine the structure of these defects with the lattice image technique in several studies on niobium oxides. This work was further refined (*8*) with ultrahigh resolution microscopy and, from the detailed structure of disordered shear planes (Wadsley defects), it is now clear that much support exists for the building-block model of these transition-metal oxides (the translation operation).

The tetragonal tungsten bronze structure, and several others, were very elegantly derived by Hyde and Bursill (*9*, *10*) by their rotation operation. Isolated rotation faults were also proposed by these authors (*10*) to exist in crystals, and they could also interpret certain observations by electron microscopy in this way later on (*11*).

Chemical twinning (reflection plus some-

0022-4596/78/2312-0191$02.00/0

times glide) was proposed as a structure building operation and many examples of structures have been classified according to this principle (*12*). Using electron microscopy it was possible to confirm this prediction, crystals of Ru_4Si_3 and V_4As_3 have been found to be rich in defects of the chemical twin type (*13, 14*). The twinning principle was recently extended to trillings (*1*) and fourlings (*15*) and also to swinging twinning (*16*). An elegant and extended application of the twin principle was recently demonstrated (*17*) for certain alloys.

We wish now to report how some tetrahedrally close-packed structures can be derived from a simple structure type, the β-tungsten structure, using the operations referred to above. The β-tungsten structure, hereafter typified by Cr_3Si, cannot be accurately represented by regular polyhedra, and must be regarded as one of the densest of structures with an average coordination number (ACN) of 13.5 (hcp and ccp have CN = 12). Regular tetrahedra cannot fill space, irregular ones can of course, and do so in Cr_3Si structure. In the bcc W structure, all atoms have the same coordination number, CN = 14, and the tetrahedra are distorted just to fill space. In Cr_3Si there are two different CN's, 14 and 12, and tetrahedra here are distorted in order to fill space as well as to accommodate atoms of two different sizes. The Cr_3Si structure contains endless strings of chromium atoms strongly bonded to each other. This character is so pronounced that we have recently described the structure as a rod structure (*18*), with its packing given in Fig. 1. Each rod contains the chromium atoms, as demonstrated in Fig. 2. The Si atoms are situated in the interstices formed by the rod packing. These interstices can be called rod-octahedra, with each rod-octahedral corner occupied by two chromium atoms giving the well-known icosahedral configuration of chromium atoms around each silicon. With this description of the structure, it is easily related to other structures like a primitive cubic structure, ω-phases, the garnet structure, etc., as was reported recently (*18*).

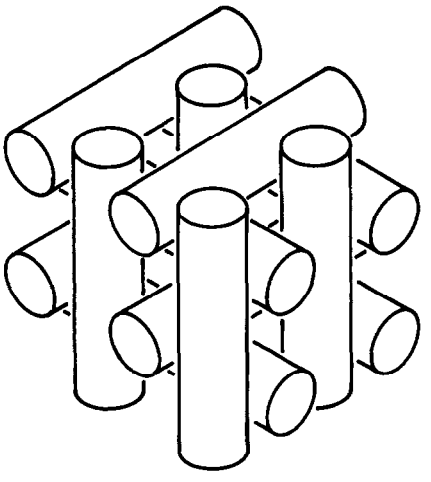

FIG. 1. Rod packing of Cr_3Si.

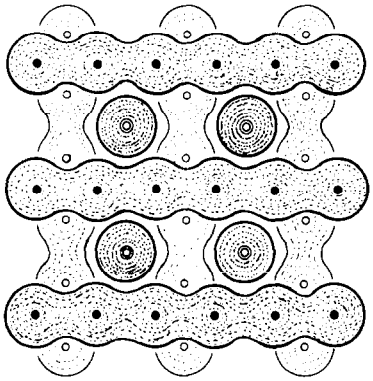

FIG. 2. Projection of rod packing in Cr_3Si. Filled and open circles are Cr on $\frac{1}{2}$ and 0, respectively. Double circles two Cr on $\frac{1}{4}$ and $\frac{3}{4}$.

In order to relate Cr_3Si to other complex alloy structures we have chosen another description which is demonstrated in Fig. 3a. The shaded regions demonstrate what Schubert (*19*) calls *Tetraederstern*, and represented in this way it is easy to see how regular crystallographic shear (*CS*) can be applied to the structure. In Cr_3Si the "tetraedersterns" are joined by corner sharing and, if the structure is sheared so that "tetraedersterns" share edges, the Zr_4Al_3 structure (*20*) is obtained. This of course involves the regular omission of atoms in the shear plane, and is exactly analogous to the construction of

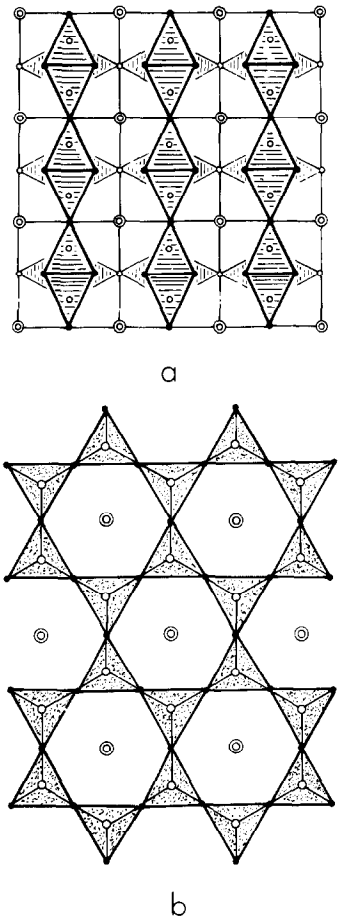

FIG. 3. (*a*) Cr_3Si. Within each square a tetraederstern. Cr as in Fig. 2. Si atoms on 0 or ½ where tetraedersterns share corners. (*b*) Zr_4Al_3, projection along *c*. The drawing after Ref. (*20*). Zr are double open circles, filled circles are Al.

Nb_3O_7F and *R*–Nb_2O_5 from the ReO_3 structure type (*26*). The *CS* operation is shown in Fig. 4 with the idealized Zr_4Al_3 in the upper right corner. If this idealized structure is projected along another axis, the *c*-axis of the real Zr_4Al_3 structure, the structure given in Fig. 5 is obtained. The real structure of Zr_4Al_3 is given in Fig. 3b, and if the two structures are compared it is easy to see that the difference between the two involves only a small distortion.

Figure 6 gives the real structure of Zr_4Al_3 and it is easy to identify the Cr_3Si blocks. Vertically in the drawing the Cr_3Si blocks are joined by tetraedersterns sharing corners. If a new, identical *CS* operation is carried out perpendicular to the first one, the $CuAl_2$ or Fe_2B structure is obtained. This is shown in Fig. 7, with the shear plane indicated by dotted lines in the left-hand idealized Zr_4Al_3 structure. Parameters calculated for the Fe_2B structure, using the Cr_3Si structure, become:

$$c/a = 2(2)^{1/2}/3 = 0.94,$$

8 Fe in 8(*h*) *I4mcm*, $x = 0.167$.

The observed parameters from the structure (*21*) are $c/a = 0.83$ and $x = 0.167$.

With these principles it is easy to design structures intermediate between Cr_3Si and Fe_2B. In terms of building blocks Fe_2B can be described as consisting of blocks of Cr_3Si 1 × 1, the hypothetical structure of Fig. 8 is then 2 × 1 and the structure of Mo_3CoSi (*22*) in Fig. 9 is clearly 2 × 2. One such 2 × 2 column is shown in Fig. 9 by denser shading. The structure of Mo_3CoSi is thus built of Cr_3Si columns sharing tetraederstern edges across two mutually perpendicular shear planes. In the intersections, units of the Fe_2B structure can be traced, and the analogy with *M*–Nb_2O_5 (*23*) or $W_3Nb_{14}O_{44}$ (*24*) is obvious. The parameters for Mo_3CoSi are given in Table I.

The structures of Mg_5Ga_2 (*25*) and MgGa (*25*) are very similar to Cr_3Si. Mg_5Ga_2 in Fig. 10A can be described as infinite Cr_3Si layers, which, if they are joined, with omission of atoms, transform the structure to the Cr_3Si type. The transformation path is shown by arrows. MgGa and Cr_3Si are shown in Fig. 10B, and simple shear operations transform one structure into another.

Rotation

The structure of W_5Si_3 (*30*) can be accurately derived by means of the Hyde rotation operation (*9*, *10*) on the Cr_3Si structure. In Fig. 11a the structure of Cr_3Si is drawn with the unit cell marked with broken lines. If cylinders of atoms, marked with

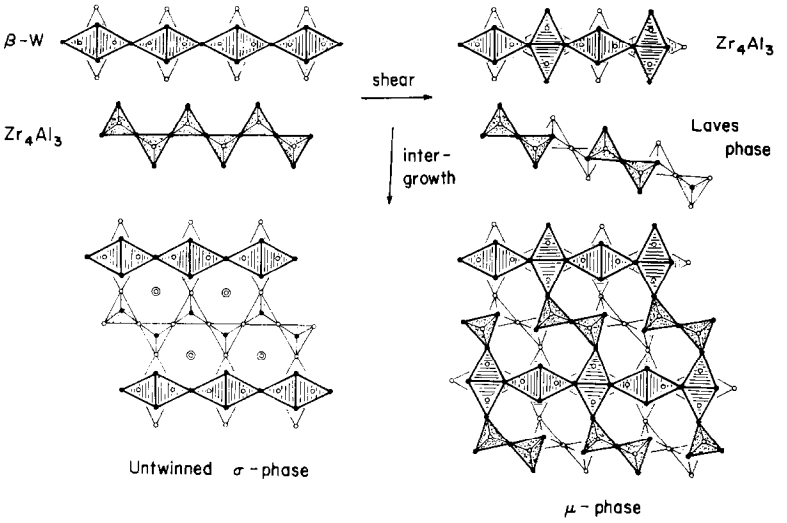

FIG. 4. The principles of shear and intergrowth in tetrahedrally close-packed structures. Structures to right idealized.

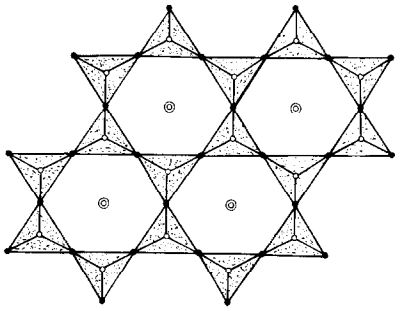

FIG. 5. Idealized Zr_4Al_3, projection along *c*.

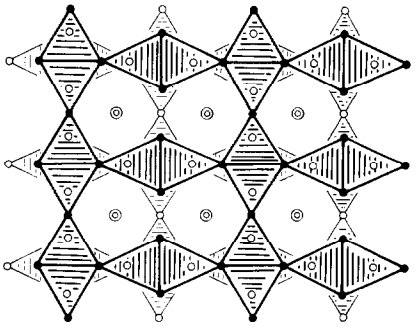

FIG. 6. The real structure of Zr_4Al_3, projection down [110]. Open and filled circles on 0 or $\frac{1}{2}$. Double circles, two Al on $\frac{1}{4}$ and $\frac{3}{4}$. Al is also situated where tetraedersterns share corners. The rest is Zr.

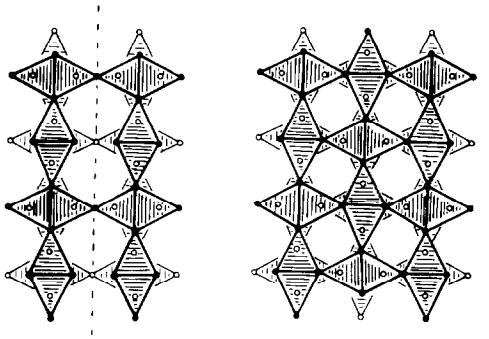

FIG. 7. Zr_4Al_3 (idealized) to left, Fe_2B to right. Dotted line is shear plane.

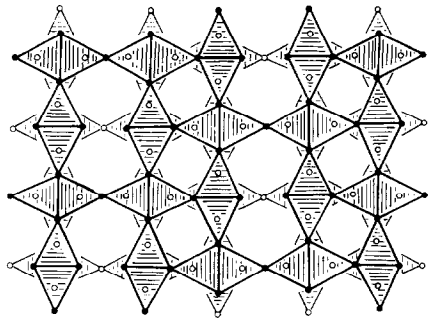

FIG. 8. Hypothetical structure, geometrically between Fe_2B and Cr_3Si.

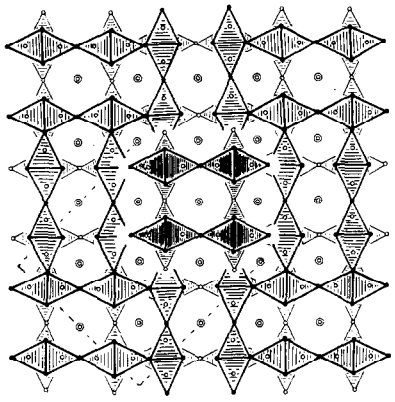

FIG. 9. Mo_3CoSi. Columns of rods of Cr_3Si, one such column heavily shaded in the center. Atoms on 0 or $\frac{1}{2}$, double circles are atoms on $\frac{1}{4}$ and $\frac{3}{4}$. The figure is constructed from Cr_3Si units, but it is not possible to distinguish it from the real structure in the scale of this drawing.

TABLE I

Calculated	Observed (*22*)
$c/a = 2(2)^{1/2}/7 = 0.404$	$c/a = 0.387$
$x_1 = 0.143$	0.155
$y_1 = 0.071$	0.085
$x_2 = 0.071$	0.067
$y_2 = 0.286$	0.294
$x_3(8h) = 0.143$	0.138
$y_3 = 0.643$	0.638

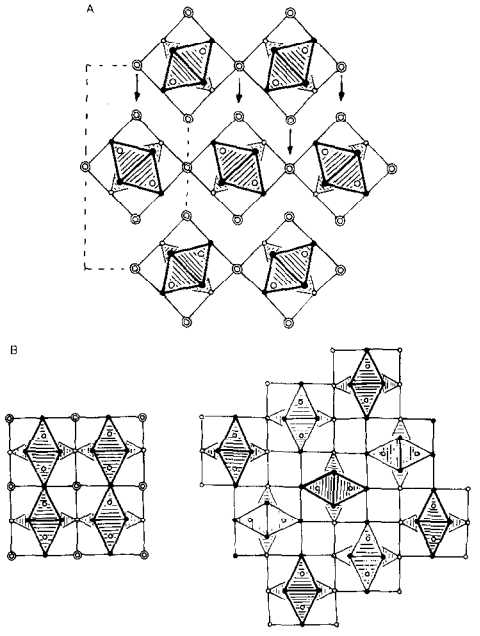

FIG. 10. (A) Ga_2Mg_5. Open and filled atoms on 0 and $\frac{1}{2}$. Double circles are two Mg on $\frac{1}{4}$ and $\frac{3}{4}$. Larger circles are also Mg. If one sheet of Cr_3Si-type layers is shifted according to arrows, the Cr_3Si-type structure is obtained. (B) GaMg, idealized (to right) is compared with Cr_3Si. The slip operation is obvious.

circles, are rotated 45° so that the shaded regions obtain the orientations shown in Fig. 11b a structure very close to that of W_5Si_3 is obtained. The structure in Fig. 11 is tetragonal as W_5Si_3, and calculated and observed parameters are given below:

	calc: $c/a = 0.500$	obs: $c/a = 0.515$
16 W in 16(*k*)	$x = 2^{1/2}/16 = 0.088$; $y = \frac{1}{2} - (3(2)^{1/2}/16) = 0.235$	$x = 0.074, y = 0.223$,
8 Si in 8(*h*)	$x = 1/4(2)^{1/2} = 0.177$	$x = 0.17$.

During the operation atoms in 4(*b*) (double circles in Fig. 11) stay in position. A doubling of the unit cell of Cr_3Si in two directions is also the result of this clockwise and anticlockwise rotation.

Another Hyde rotation operation in Cr_3Si produces the structures of α- and β-V_3S (*27*). The structure types are Ni_3P (*28*) and β-V_3S and the structural chemistry of isostructural compounds have been discussed by Rundqvist (*29*). The two structures, given in Fig. 12, are very similar. Only a translation of $\frac{1}{2}c$ of the atoms in the corners of the Cr_3Si squares transforms α- into β-V_3S. Another way to do this is by rotation; if the atom columns within circles are rotated 45° α-V_3S goes to β-V_3S. On the other hand, if atom columns within circles in β-V_3S are rotated 45°, and if the corner atoms of the tetraedersterns are translated $\frac{1}{4}c$ and shifted somewhat so that they overlap, a structure which topologically is the

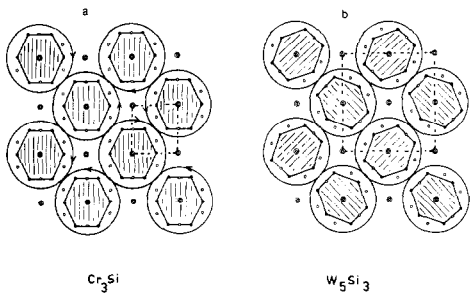

FIG. 11. Rotation mechanism for transforming the Cr_3Si structure type to the W_5Si_3 structure type.

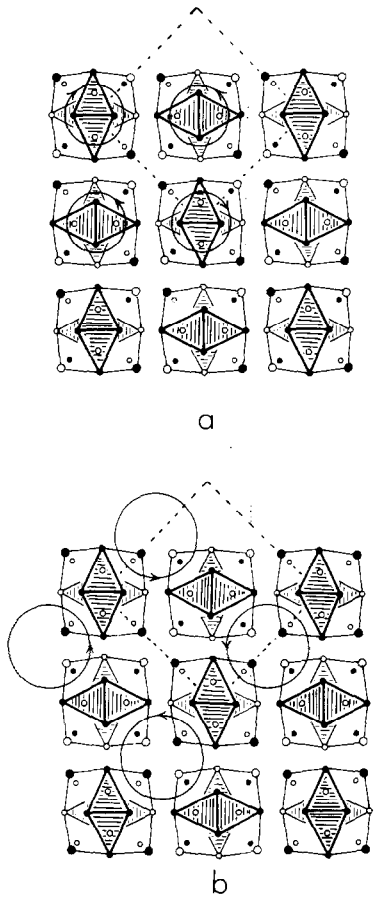

FIG. 12. (a) β-V_3S. Small and big, open and filled circles are S and V on 0 and $\frac{1}{2}$; medium-sized circles, V on $\frac{1}{4}$ and $\frac{3}{4}$. (b) α-V_3S. Small and big, open and filled circles are S and V on 0 and $\frac{1}{2}$; medium-sized circles, V on $\frac{1}{4}$ and $\frac{3}{4}$. Circles show rotation mechanism for transforming these structures to Cr_3Si.

same as Cr_3Si, is obtained. This is indeed a simple mechanism and it is important to mention that the A and B atoms in A_3B (V_3S or Cr_3Si) remain ordered during the transformation

Tetrahedrally Close-Packed Structures

Friaur–Laves Phases and Related Structures

The basic geometry of some of the structures shown below was described by Frank and Kasper in a very elegant way (*31*, *32*). However, analysis of some structures, notably the ν- and χ-phases seem to resist the classification, and we will describe how these and other structures can be derived with operations used above.

Going back to Fig. 4 in the upper left corner, a string of tetraedersterns share corners and represent the Cr_3Si structure. Underneath is a string of the real Zr_4Al_3 structure (projected along c). If Zr_4Al_3 is sheared again to give the string of edge-shared trigonal bipyramids, shown in the right part of Fig. 4, second from top, a part of the Cu_2Mg structure is obtained. This operation increases to 16 the coordination number for atoms in the shared edges of trigonal bipyramids, and, in the real structure of Cu_2Mg, these positions are also occupied by the larger Mg atoms. This causes the real structure, although topologically the same as shown in Fig. 13, to

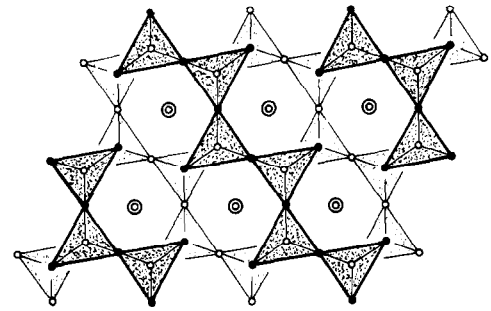

FIG. 13. $MgCu_2$ (the real structure) projected along [1$\bar{1}$0]. Mg on 0 or $\frac{1}{2}$, situated in centers of truncated tetrahedra, or where trigonal bipyramids share edges. Cu, in 0 or $\frac{1}{2}$, where trigonal bipyramids share corners. Double circles, two overlapping Cu on $\frac{1}{4}$ and $\frac{3}{4}$.

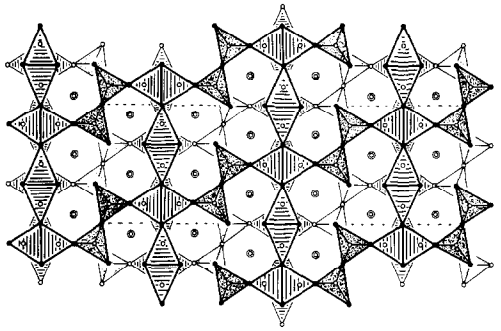

FIG. 14. μ-phase, W_6Fe_7. Projection along [110], filled and open circles atoms on 0 and ½. Double circles are two Fe on ¼ and ¾. Fe is also where trigonal bipyramids share corners, and where tetraedersterns share corners with trigonal bipyramids. W situated where trigonal bipyramids share edges, and in the corners of the central tetrahedron of the tetraederstern. The drawing is constructed from Zr_4Al_3 and $MgCu_2$, but impossible to distinguish from the real structure.

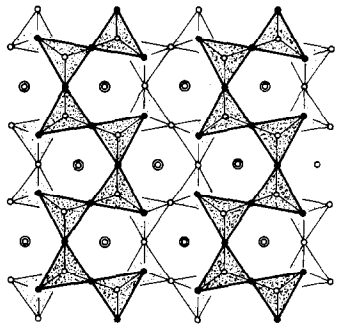

FIG. 15. $MgZn_2$, real structure. Ordering and heights of atoms as in $MgCu_2$, Fig. 13. Projection along [110].

be slightly modified. The cubic Cu_2Mg can also be derived from ccp by the systematic substitution of two ccp atoms by one Mg. The coordination polyhedron around Mg is the truncated tetrahedron. Such truncated tetrahedra share faces in the Friauf–Laves phases and each Mg will have four other Mg atoms as next neighbors in the centers of four other truncated tetrahedra. This increases the CN of Mg to 16, and such four-capped truncated tetrahedra are called Friauf polyhedra.

In Fig. 4 is also shown how a part of Cu_2Mg (idealized) can grow together with idealized Zr_4Al_3 to form the μ-phase. In Fig. 14 the μ-phase is constructed by letting sheets of the real structures of Cu_2Mg and Zr_4Al_3 intergrow. No parameters were calculated, but within the accuracy given by the drawing the constructed structure is identical with the real structure of the μ-phase.

Another Laves phase, the $MgZn_2$ compound, can analogously be derived from hcp and be described as the packing of truncated tetrahedra. It is derived equally well by twinning the Mg_2Cu structure, and the calculated parameters according to that operation are:

$$c/a = 2(2)^{1/2}/3^{1/2} = 1.633,$$

$z_{Mg} = \frac{1}{16} = 0.0625$, and $x_{Zn} = \frac{1}{6} = 0.1667$. Observed parameters are $c/a = 1.648$, $z = 0.062$, and $x = 0.17$, respectively. The structure is given in Fig. 15.

It is easy to see from Figs. 13 and 15 that these two structures both can be sheared once more. The sheared structure of Cu_2Mg is shown in Fig. 16 and the "tunnels" are now relatively small. The coordination number of atoms are lowered, being 9 and 11 for the two independent atoms in the unit cell. The structure is not tetrahedrally close-packed, and the search for a representative has to be done in other fields of structures. The group of interstitial alloys that have trigonal prisms as hosts for interstitial atoms, have generally lower coordination numbers for atoms. The structure of W_2CoB_2 (*34*) is topologically the same as this sheared version of Cu_2Mg with boron atoms entering the "tunnels." This structure, and consequently also W_2CoB_2, can be transformed to hcp by a new simple shear

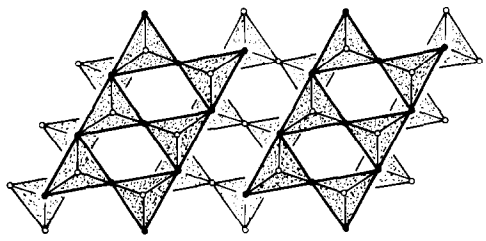

FIG. 16. Sheared structure of $MgCu_2$, topologically the same as W_2CoB_2.

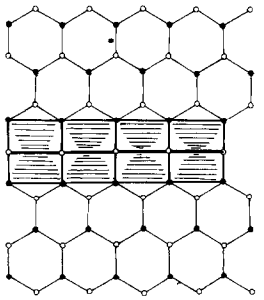

FIG. 17. Planar fault of rhombic prisms in hcp.

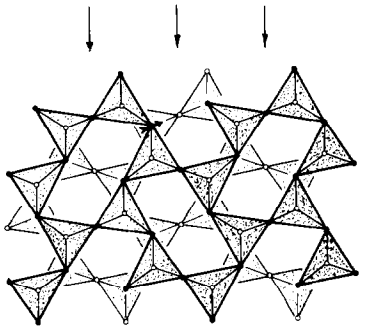

FIG. 18. Sheared structure of $MgZn_2$. Small arrow gives shift 0.13 Å to transform the structure of Ga. Larger arrows indicate twin planes for transforming the structure to CeAl.

operation, and in Fig. 17 we show how a chain of trigonal prisms, or, equally well, rhombic prisms (*35*), occurs as an extended planar fault in hcp.

The sheared structure of $MgZn_2$ is shown in Fig. 18. It is interesting to find that the metal-atom positions in this structure agree very well with the positions of anions and lone pairs of electrons in *L*–SbOF (*36*). The two nets are compared in Fig. 19.

The space group for this sheared $MgZn_2$ (AB_2) structure is *Cmca*, with atoms 8 *A* in 8(*f*), with $y = \frac{1}{10}$ and $z = \frac{1}{8}$, and with 4*B* in 4(*b*). This structure is very similar to the structure of stable gallium. If the *A* atoms are shifted 0.13 Å in the direction of the arrow in Fig. 18 (this shifts the *y* and *z* parameters to 0.081 and 0.1549, respectively), the *A* atoms are in the positions of the gallium atoms in the metal structure. The $a:b:c$ ratio for sheared $MgZn_2$ is $2^{1/2}:5(3)^{1/2}/6:3^{1/2}$ or 0.98 : 1 : 1.697 and for gallium it is 0.999 : 1 : 1.693. The only real difference between the two structures is the *B* atoms; if they are removed, the structures virtually become identical. Ordered metal-atom vacancies of this kind are to our knowledge unusual but do occur in the $MgGa_2$ structure (*39*). Pearson (*40*) points out that if these vacancies are occupied by atoms, the structure of $MgGa_2$ can be described as a regular network of pentagons and triangles. However, the X-ray work by Smith *et al.* (*39*) clearly indicates that no extra atoms are present. These observations need an explanation and it is convenient to assume localization of extra electrons, possible s_2 pairs, to fill these holes in the structures of gallium and $MgGa_2$. Support for this is also given by the unusual behavior of gallium at its melting point. The volume and electrical resistivity increase in going from the melt to the solid phase, and according to Mott (*41*), the effective number of free electrons increases by a factor of about 10 when gallium melts. The structure of metastable gallium (*42*), prepared from a supercooled melt, has a more normal metal structure. It has the same structure as the chromium atoms in CrB, with

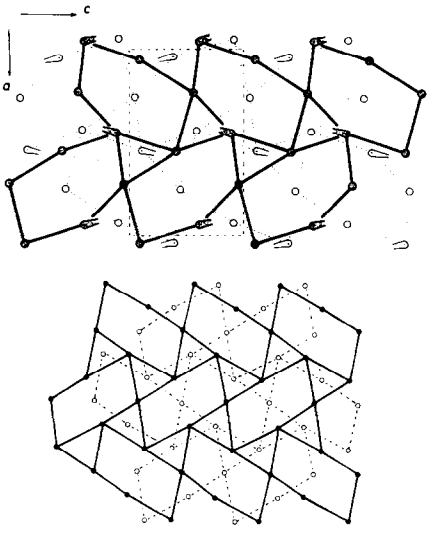

FIG. 19. Net of atoms of structure of Fig. 18, compared with net of anions and lone pairs in *L*–SbOF.

a CN of 10 compared with 7 for the gallium atoms in stable gallium. Naturally the metastable gallium reflects more the liquid state and the localization of electrons to ordered positions in stable gallium causes the unique electrical properties and the well-known volume decrease at melting. The lone pairs in ionic compounds of the s^2 elements are attached to their cations (*37*, *38*), but the analogy in description and classification of structure is obvious.

Sheared $MgZn_2$ can be twinned at the planes indicated by arrows in Fig. 18. The polyhedra created in the twin plane by this operation are pentagonal antiprisms, and the structure is topologically the same as CeAl (*43*).

The χ, σ, P, M $(Co_{0.57}Si_{0.43})_3V_2$ and ν-Phases

Fourling operations were recently suggested for the construction of structures, and some applications were demonstrated (*15*, *44*). The complex structure of the χ-phase (*45*, *46*) is easily understood if it is dissected to fourling units. In Fig. 20 the structure is drawn as a fourling of $MgZn_2$ (compare Fig. 15) and such, somewhat elliptical, units are shaded and surrounded by thin lines in the figure. The fourling operation is easy and accurate to make, as the reader can convince himself by the use of transparent paper and Fig. 15. The operation creates empty space along the fourling axis; in the crystal this space is stuffed with extra atoms to form a tetraederstern. In a rather large drawing, fourling units of the exact structure of $MgZn_2$ were used, and atomic coordinates for this constructed structure of the χ-phase were measured directly on the drawing. The agreement between these coordinates and those observed (*46*) is surprisingly good as shown in Table II.

In the lower left part of Fig. 4 it is shown how Cr_3Si and Zr_4Al_3 can intergrow and form a so far unknown structure. If this structure is twinned the well-known σ-phase structure (*47*) is obtained and given in Fig. 21, where also the twin planes are shown with arrows. In this case the atomic parameters have been calculated by the twin operation and in Table III they are compared with those actually observed. The twin block size can be varied, and an

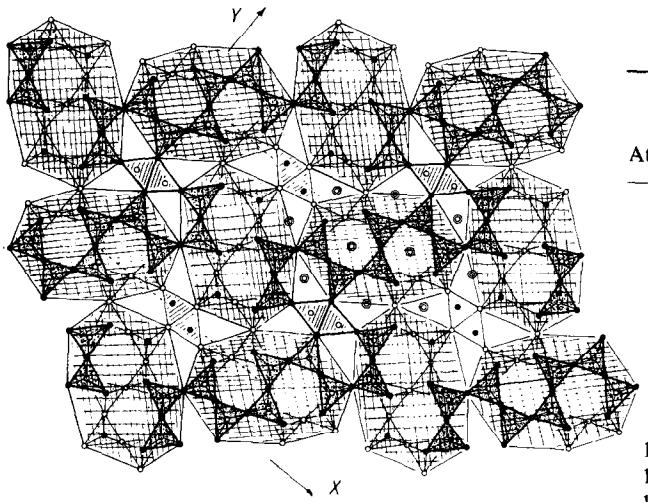

FIG. 20. The structure of the χ-phase, constructed from fourling units (shaded and surrounded by thin lines) of $MgZn_2$. The drawing is not possible to distinguish from the real structure. Atoms on 0 and ½, except double circles which are two atoms overlapping on ¼ and ¾.

TABLE II

THE χ-PHASE[a]

	Measured		Observed	
Atom	*x*	*y*	*x*	*y*
1	0.113	0.093	0.111	0.086
2	0.179	0.400	0.176	0.398
3	0.394	0.219	0.398	0.210
4	0.057	0.276	0.055	0.278
5	0.232	0.216	0.236	0.213
6	0.214	0.00	0.216	0.992
7	0.358	0.061	0.361	0.057
8	0.500	0.310	0.499	0.311
9	0.338	0.403	0.339	0.399
10	0.500	0.500	½	½
14	0.074	0.534	0.070	0.529
15	0.230	0.591	0.235	0.587
16	0.350	0.749	0.355	0.742
17	0.206	0.808	0.209	0.802
18	0.051	0.909	0.051	0.903

[a] *a*/*b* (obs) = 1.24; *a*/*b* (meas) = 1.23.

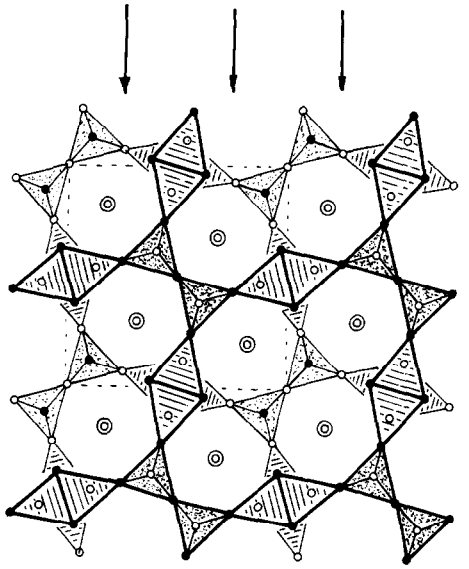

FIG. 21. The σ-phase structure. Arrows indicate twin planes. The drawing is constructed from a twin operation, but it is not possible to distinguish it from the real structure.

TABLE III[a]

THE σ-PHASE

Atom	calc.	obs.
B.	$x = 0.390$	0.398
C.	$x = 0.461$	0.463
	$y = 0.125$	0.132
D.	$x = 0.750$	0.738
	$y = 0.067$	0.065
E.	$x = 0.183$	0.182

[a] $(a/c)_{calc} = (2 + 3^{1/2})^{1/2} = 1.93$; $(a/c)_{obs} = 1.94$.

example of this is given in Fig. 22 as a hypothetical structure.

The structure of the σ-phase can be used to derive the *P*-structure (*48*). In Fig. 23 a part of the σ-phase is drawn in the right part and if this part is twinned and sheared, the *P*-phase structure is obtained. The σ-phase blocks are indicated in the figure. Measured coordinates, obtained as in the χ-phase case, are in good agreement with the observed ones and compared in Table IV. The structure can also be derived by twinning the μ-phase structure.

The so-called *M*-phase (*49*) can be obtained

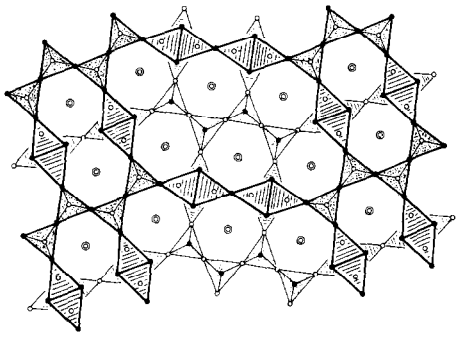

FIG. 22. The twin blocks of Fig. 21 have been expanded, so that larger units of the untwinned hypothetical structure of Fig. 4 are obtained. Hypothetical structure.

by a crystallographic shear operation from the *P*-phase. In Fig. 24, however, it has been derived by twinning plus shear of the μ-phase structure. The extension and overlap (shear) of the μ-phase blocks are shown with arrows in the figure. The measured and observed parameters are again very good and compared in Table V.

The relatively simple structure of $(Co_{0.57}Si_{0.43})_3V_2$ (*50*) is easily derived through a perpendicular intergrowth of the μ-phase structure and $MgZn_2$, as demonstrated in Fig. 25. The only atoms not generated by this construction are the two in the special position $2d$ $(0\ \frac{1}{2}\ \frac{1}{2})$. A very accurate structure is derived as shown in Table VI where the measured and observed parameters are compared.

The complex structure of the so-called ν-phase (*51*) is shown in Fig. 26. The structure contains large units of the σ-phase, marked with dotted trigonal bipyramids and shaded tetraedersterns. The σ-columns are intergrown along a with Zr_4Al_3, and such σ-phase-Zr_4Al_3 blocks are intergrown in the b-direction with a twinned μ-phase structure.

Conclusions

The observations made in this article call for experiments with high-resolution electron microscopy in order to reveal whether the

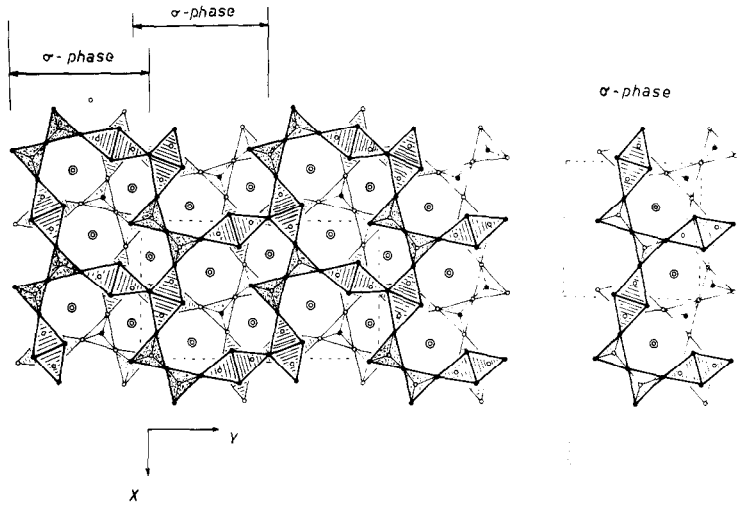

FIG. 23. The *P*-phase structure. To the right is shown the σ-phase structure, which is used in twin and shear operations to produce this *P*-phase drawing.

TABLE IV[a]

THE *P*-PHASE

Atom	Measured		Observed	
	x	*y*	*x*	*y*
1	0.069	0.104	0.074	0.113
2	0.130	0.249	0.136	0.255
3	0.329	0.141	0.326	0.158
4	0.600	0.180	0.606	0.182
5	0.681	0.338	0.665	0.325
6	0.483	0.460	0.475	0.454
7	0.188	0.409	0.199	0.405
8	0.814	0.068	0.815	0.078
9	0.949	0.375	0.938	0.365
10	0.511	0.035	0.520	0.036
11	0.251	0.541	0.250	0.537
12	0.371	0.289	0.386	0.288

[a] $(b/a)_{meas} = 1.76$; $(b/a)_{obs} = 1.87$.

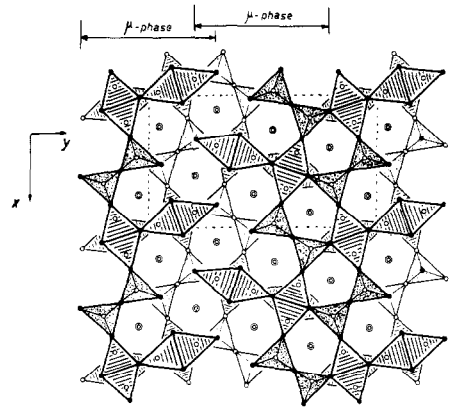

FIG. 24. The *M*-phase structure. It is generated by twinning and shear of the μ-phase structure, blocks of which are shown between arrows. The structure of the drawing is very similar to the real structure.

ideas proposed are realistic or not. Such studies would also be fruitful when relating the nature of defect crystals with a physical property like conductivity.

The Cr_3Si structure type is common for many compounds which are good superconductors. The structural property of three-dimensional nonconnecting rods of atoms with strongly directional bonds is obviously one explanation for the superconductivity. In several of the complex structures described in this article the rod-structure feature of Cr_3Si has been broken and exist only in two or one dimensions. Naturally we expect the defect structure of Cr_3Si-type crystals to be very complex, but in such studies we can be guided by the related structures discussed in this article, and which are derived by means of shear, rotation, twin, and intergrowth operations on Cr_3Si.

TABLE V[a]

THE *M*-PHASE

Atom	Measured		Observed	
	x	*y*	*x*	*y*
1	0.062	0.147	0.059	0.149
2	0.294	0.398	0.299	0.389
3	0.521	0.539	0.524	0.541
4	0.613	0.696	0.616	0.707
5	0.027	0.446	0.014	0.448
6	0.829	0.296	0.839	0.294
7	0.070	0.626	0.071	0.623
8	0.329	0.672	0.326	0.670
9	0.828	0.579	0.817	0.578
10	0.118	0.295	0.112	0.295
11	0.264	0.541	0.255	0.545

[a] $(b/a)_{meas} = 1.75$; $(b/a)_{obs} = 1.75$.

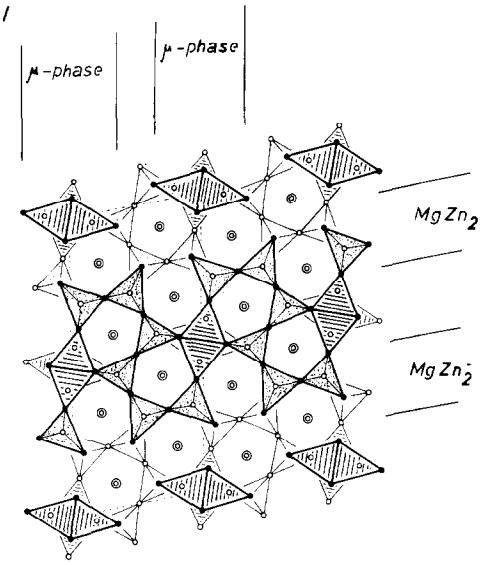

FIG. 25. The $(Co_{0.57}Si_{0.43})_3V_2$ structure. The perpendicular intergrowth of blocks of μ-phase and $MgZn_2$ shown with arrows. The drawing constructed, but not possible to distinguish from the real structure.

With the classification system used it is easy to derive many new hypothetical structures. Whether it is possible to make these is a matter of speculation at the moment. We know that atomic size is one important parameter and it is interesting to calculate average coordination number (ACN) for various phases (compare Ref. (*53*)):

Cr_3Si, ACN 13.50

Shear phases	*ACN*	*Twin phases*	*ACN*
Zr_4Al_3	13.43	σ-phase	13.47
Mo_3CoSi	13.43	χ-phase	13.35
Fe_2B	13.33		
Laves phase	13.33		
Intergrowth	*ACN*	*Twin + shear phases*	*ACN*
untwinned σ (hypothetical)	13.38	*M*phase	13.38
μ-phase	13.38	*P*-phase	13.43
$(Co_{0.57}Si_{0.43})_3V_2$	13.36		
ν-phase	13.44	*Rotation* *ACN*	
		W_5Si_3 13.0	

The CN for atoms in these complex structures is easily found using the coding system of Pearson and Shoemaker (*52*). The general trend in ACN is that shear and rotation operations cause lower ACN while twinning has the opposite effect. Intergrowth gives an average in ACN of the two structures intergrowing. The ν-phase has a rather high ACN, which of course reflects the very big units of σ-phase in the structure. The μ-phase and Laves-phase components in *M* and *P* are rather large and would give a low ACN, but ACN is increased by twin operations. It is probable that high temperature would favor

TABLE VI

$(Co_{0.57}Si_{0.43})_3V_2$

	Measured		Observed	
Atom	x	y	x	y
1	0.054	0.356	0.048	0.367
2	0.208	0.550	0.208	0.562
3	0.208	0.929	0.208	0.932
4	0.470	0.818	0.473	0.817
5	0.067	0.979	0.069	0.981
6	0.291	0.265	0.287	0.267
7	0.371	0.549	0.374	0.543
8	0.378	0.054	0.375	0.042
9	0.167	0.227	0.160	0.226
10	0.085	0.700	0.088	0.695

[a] $(a/b)_{meas} = 2.18$; $(a/b)_{obs} = 2.27$.

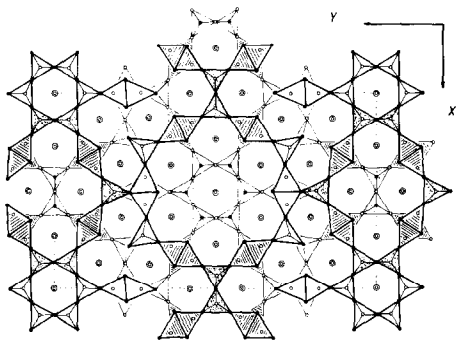

FIG. 26. The real structure of the ν-phase. The large elliptical units of σ-phase structure are shaded and dotted.

shearing while low temperature and high pressure would favor twinning. The Hyde rotation mechanism for transforming α- and β-V_3S to the Cr_3Si type is of special interest. Surely such a phase transformation would be favored by high pressure, and new superconducting material could be prepared. For example, Mo_3P of the Ni_3P type is already a good superconductor with $T_c = 7.0°K$ and if it could be transformed to a Cr_3Si structure type it might have a considerably higher T_c.

Acknowledgment

This work was supported by the Swedish National Science Research Council.

References

1. B. G. HYDE, A. N. BAGSHAW, S. ANDERSSON, AND M. O'KEEFFE, *Annu. Rev. Mat. Sci.* **4**, 43 (1974).
2. S. ANDERSSON, *Bull. Soc. Chim.*, 1088 (1965).
3. R. S. ROTH AND A. D. WADSLEY, *Acta Crystallogr.* **19**, 42 (1965).
4. S. ANDERSSON AND A. D. WADSLEY, *Acta Crystallogr.* **15**, 194 (1962).
5. S. ANDERSSON, *Ark. Kemi* **26**, 521 (1967).
6. S. ANDERSSON, *Z. Anorg. Chemie.* **366**, 96 (1969).
7. J. G. ALLPRESS, J. V. SANDERS, AND A. D. WADSLEY, *Acta Crystallogr.* **1325**, 1156 (1969).
8. S. IIJIMA, *J. Appl. Phys.* **42**, 5891 (1971).
9. B. G. HYDE, *in* "Proceedings of the 7th International Symposium on the Reactivity of Solids, 1972," Chapman and Hall, London (1972).
10. L. A. BURSILL AND B. G. HYDE, *Nature Phys. Sci.* **240**, No. 102, 122 (1972).
11. S. IIJIMA AND J. G. ALLPRESS, *Acta Crystallogr., Sect. A* **30**, 22, 29 (1974).
12. S. ANDERSSON AND B. G. HYDE, *J. Solid State Chem.* **9**, 92 (1974).
13. S. ANDERSSON, C. LEYGRAF, AND T. JOHNSSON, *J. Solid State Chem.* **14**, 78 (1975).
14. S. ANDERSSON, H. ANNEHED, L. STENBERG, AND R. BERGER, *J. Solid State Chem.* **19**, 169 (1976).
15. J.-O. BOVIN AND S. ANDERSSON, *J. Solid State Chem.* **18**, 347 (1976).
16. J.-O. BOVIN AND S. ANDERSSON, *J. Solid State Chem.* **20**, 127 (1977).
17. E. PARTHÉ, *Acta Crystallogr., Sect. B* **32**, 2813 (1976).
18. M. O'KEEFFE AND S. ANDERSSON, in print.
19. K. SCHUBERT, "Kristallstrukturen zweikomponentiger Phasen," p. 150, Springer–Verlag, New York/Berlin (1964).
20. C. G. WILSON, D. K. THOMAS, AND F. J. SPOONER, *Acta Crystallogr.* **13**, 56 (1960).
21. G. HÄGG, *Z. Phys. Chem. Abt. B* **11**, 152 (1930).
22. E. J. GLADYSEVSKIJ, P. I. KRIPJAKEVIC, AND R. V. SKOLOZDRA, *Dokl. Akad. Nauk SSSR* **175**, 1047 (1968).
23. W. MERTIN, S. ANDERSSON, AND R. GRUEHN, *J. Solid State Chem.* **1**, 419 (1970).
24. R. S. ROTH AND A. D. WADSLEY, *Acta Crystallogr.* **19**, 32 (1965).
25. K. SCHUBERT, F. GAUZZI, AND K. FRANK, *Z. Metallk.* **54**, 422 (1963).
26. S. ANDERSSON, *Acta Chem. Scand.* **18**, 2339 (1964).
27. B. PEDERSEN AND F. GRØNVOLD, *Acta Crystallogr.* **12**, 1022 (1959).
28. B. ARONSSON, *Acta Chem. Scand.* **9**, 137 (1955).
29. S. RUNDQVIST, *Ark. Kemi* **20**, 67 (1962).
30. B. ARONSSON, *Acta Chem. Scand.* **9**, 1107 (1955).

31. F. C. FRANK AND J. S. KASPER, *Acta Crystallogr.* **11**, 184 (1958).
32. F. C. FRANK AND J. S. KASPER, *Acta Crystallogr.* **12**, 483 (1959).
33. S. SAMSON, *in* "Structural Chemistry and Molecular Biology," p. 687, Freeman, San Francisco (1968).
34. W. REIGER, H. NOWOTNY, AND F. BENESOVSKY, *Mh. Chem.* **97**, 378 (1966).
35. H. NYMAN, *J. Solid State Chem.* **17**, 75 (1976).
36. A. ÅSTRÖM AND S. ANDERSSON, *J. Solid State Chem.* **6**, 191 (1973).
37. S. ANDERSSON, A. ÅSTRÖM, J. GALY, AND G. MEUNIER, *J. Solid State Chem.* **6**, 187 (1973).
38. J. GALY, G. MEUNIER, S. ANDERSSON, AND A. ÅSTRÖM, *J. Solid State Chem.* **13**, 142 (1975).
39. G. S. SMITH, K. F. MUCKER, Q. JOHNSON, AND D. H. WOOD, *Acta Crystallogr., Sect. B* **25**, 549 (1969).
40. W. B. PEARSON, "The Crystal Chemistry and Physics of Metals and Alloys," p. 744, Wiley, New York (1972).
41. N. F. MOTT, *Proc. Roy. Soc. Ser. A* **146**, 465 (1934).
42. H. CURIEN, A. RIMSKY, AND A. DE FRAIN, *Bull. Soc. Fr. Mineral. Cristallogr.* **84**, 260 (1961).
43. C. BÈCLE AND R. LEMAIRE, *Acta Crystallogr.* **23**, 840 (1967).
44. J.-O. BOVIN, *Acta Crystallogr., Sect. B* **32**, 1771 (1976).
45. Y. P. YARMOLUK, P. I. KRIPYAKEVICH, AND E. I. HLADYSHEVSKII, *Kristallografiya* **15**, 268 (1970).
46. P. C. MANOR, C. B. SHOEMAKER, AND D. B. SHOEMAKER, *Acta Crystallogr. Sect. B* **28**, 1211 (1972).
47. B. G. BERGMAN AND D. P. SHOEMAKER, *Acta Crystallogr.* **7**, 857 (1954).
48. D. P. SHOEMAKER, C. B. SHOEMAKER, AND F. C. WILSON, *Acta Crystallogr.* **10**, 1 (1957).
49. C. B. SHOEMAKER AND D. P. SHOEMAKER, *Acta Crystallogr.* **23**, 231 (1967).
50. P. J. KRIPYAKEVICH AND Y. P. YARMOLUK, *Dopov. Akad. Nauk Ukr. RSR Ser.* 17, **10**, 948 (1970).
51. C. B. SHOEMAKER AND D. P. SHOEMAKER, *Acta Crystallogr., Sect. B* **27**, 227 (1971).
52. W. B. PEARSON AND C. B. SHOEMAKER, *Acta Crystallogr., Sect. B* **25**, 1178 (1969).
53. Y. P. YARMOLUK AND P. J. KRIPYAKEVICH, *Kristallografia* **19**, 539 (1974).